5754 *Chem. Mater.* **2010,** *22,* 5754–5761
DOI:10.1021/cm102058n

CHEMISTRY OF MATERIALS
Article

Microwave-Solvothermal Synthesis of Nanostructured Li_2MSiO_4/C (M = Mn and Fe) Cathodes for Lithium-Ion Batteries

T. Muraliganth, K. R. Stroukoff, and A. Manthiram*

Electrochemical Energy Laboratory and Materials Science and Engineering Program, The University of Texas at Austin, Austin, Texas 78712, United States

Received July 23, 2010. Revised Manuscript Received September 15, 2010

Nanostructured Li_2FeSiO_4 and Li_2MnSiO_4 cathodes have been synthesized by a facile microwave-solvothermal synthesis. To improve crystallinity and enhance electronic conductivity, the resulting samples have been mixed with sucrose and heated at 650 °C for 6 h in argon atmosphere. The Li_2MSiO_4/C nanocomposites, thus, obtained have been characterized by X-ray diffraction, scanning electron microscopy, transmission electron microscopy, Raman spectroscopy, electrochemical measurements, and differential scanning calorimetry. The Li_2FeSiO_4/C sample exhibits good rate capability and stable cycle life, with discharge capacities of 148 mAh/g at room temperature and 204 mAh/g at 55 °C. Although Li_2MnSiO_4/C shows higher discharge capacities of 210 mAh/g at room temperature and 250 mAh/g at 55 °C, it suffers from poor rate capability and drastic capacity fade. The disparity in the electrochemical performance and redox behavior between Li_2FeSiO_4/C and Li_2MnSiO_4/C can be attributed to the differences in the structural stability of the delithiated phases, Jahn−Teller distortion of Mn^{3+} ions, Mn dissolution, and electronic conductivity.

Introduction

Lithium-ion batteries have revolutionized the portable electronics market, and they are being intensively pursued for vehicle applications including hybrid electric vehicles (HEV), plug-in hybrid electric vehicles (PHEV), and electric vehicles (EV). They are also being seriously considered for the efficient storage and utilization of intermittent renewable energies like solar and wind. However, the major challenges in adopting the technology for large scale applications are the cost, safety, and cyclic stability of the currently used electrode materials. Most of the commercial lithium-ion batteries typically employ oxide cathodes such as $LiCoO_2$, $Li[Ni,Mn,Co]O_2$, and $LiMn_2O_4$ and graphite as the anode. The highly oxidized $Co^{3+/4+}$, $Ni^{3+/4+}$, and $Mn^{3+/4+}$ couples in the transition metal oxide cathodes offer a high cell voltage of ~4 V. However, these materials are prone to release oxygen from the lattice in the charged state due to the inherent chemical instability of the highly oxidized species such as Co^{4+} and Ni^{4+},[1−3] which can give rise to a thermal runaway reaction within the cell and cause heat production or fire. Recognizing these safety concerns, cathodes containing polyanions such as XO_4^{2-} (X = S, Mo, and W) were first pursued as lithium insertion/extraction hosts in the 1980s by Manthiram and Goodenough.[4,5] Replacement of the simple oxide ions by such polyanions were found to beneficially lower the redox energies of chemically more stable couples such as $Fe^{2+/3+}$ through the inductive effect and, thereby, increase the cell voltage. For example, the voltage of the $Fe^{2+/3+}$ redox couple increases from < 2.5 V in a simple oxide like Fe_2O_3 to 3.0 V in $Fe_2(MoO_4)_3$ and 3.6 V in $Fe_2(SO_4)_3$.[4,5] The highly covalent S−O and Mo−O bonds weaken the Fe−O covalency due to the inductive effect and, thereby, lower the relative position of the $Fe^{2+/3+}$ couple, resulting in higher cell voltage.

Building on this concept, several phosphates have been investigated as cathodes,[6,7] and the phospho-olivine $LiFePO_4$ has emerged as an attractive candidate.[8] Since its identification as a potential cathode, $LiFePO_4$ has been the subject of intensive studies from both scientific and technological points of view.[8−25] While Fe is

*To whom correspondence should be addressed. Phone: 512-471-1791. Fax: 512-471-7681. E-mail: rmanth@mail.utexas.edu.

(1) Chebiam, R. V.; Prado, F.; Manthiram, A. *Chem. Mater.* **2001**, *13*, 2951.
(2) Venkatraman, S.; Manthiram, A. *Chem. Mater.* **2002**, *14*, 3907.
(3) Kim, J.; Noh, M.; Cho, Kim, J. H. *J. Electrochem. Soc.* **2005**, *152*, A1142.
(4) Manthiram, A.; Goodenough, J. B. *J. Power Sources* **1989**, *26*, 403.
(5) Manthiram, A.; Goodenough, J. B. *J. Solid State Chem.* **1987**, *71*, 349.
(6) Padhi, A. K.; Nanjundaswamy, K. S.; Masquelier, C.; Okada, S.; Goodenough, J. B. *J. Electrochem. Soc.* **1997**, *144*, 1609.
(7) Padhi, A. K.; Nanjundaswamy, K. S.; Masquelier, C.; Goodenough, J. B. *J. Electrochem. Soc.* **1997**, *144*, 2581.
(8) Padhi, A. K.; Nanjundaswamy, K. S.; Goodenough, J. B. *J. Electrochem. Soc.* **1997**, *144*, 1188.
(9) Yamada, A.; Koizumi, H.; Nishimura, S.−I.; Sonoyama, N.; Kanno, R.; Yonemura, M.; Nakamura, T.; Kobayashi, Y. *Nat. Mater.* **2006**, *5*, 357.
(10) Delacourt, C.; Poizot, P.; Tarascon, J.−M.; Masquelier, C. *Nat. Mater.* **2005**, *4*, 254.
(11) Gibot, P.; Cabans, M. C.; Laffont, L.; Levasseur, S.; Carlach, P.; Hamelet, S.; Tarascon, J.−M.; Masqulier, C. *Nat. Mater.* **2008**, *7*, 741.
(12) Meethong, N.; Carter, W. C.; Chiang, Y.−M. *Electrochem. Solid-State Lett.* **2007**, *10*, A13.
(13) Huang, H.; Yin, S.−C.; Nazar, L. F. *Electrochem. Solid-State Lett.* **2001**, *4*, A170.

 Published on Web 10/01/2010

inexpensive and environmentally benign, the covalently bonded PO_4 groups offer excellent thermal stability. Despite these advantages, $LiFePO_4$ suffers from poor lithium-ion and electronic conductivities, and several strategies have been adopted in recent years to overcome this problem including cationic doping, decreasing the particle size through various synthesis methods, and coating with electronically conducting agents.[13−19] However, with a lower operating voltage of ~3.4 V, theoretical capacity of ~170 mAh/g, and lower crystallographic density, the energy density of $LiFePO_4$ is lower than that of layered $Li[Ni,Mn,Co]O_2$ oxide cathodes.[26]

In this regard, polyanion-containing frameworks that can reversibly insert/extract two lithium ions per formula unit would help to increase the capacity and energy density while benefiting from the highly stable covalently bonded XO_4 groups. Recently, the silicate Li_2FeSiO_4 that is based on LISICON (lithium super ionic conductor) structure has become appealing, as it could theoretically insert/extract two lithium per formula unit with a theoretical capacity of ~330 mAh/g.[27] Following this, silicates with the general formula Li_2MSiO_4 (M = Mn, and Co) have also been identified as potential lithium insertion/extraction hosts.[28−30] Among them, Li_2FeSiO_4 has drawn the most attention, as it exhibits a stable cycle life with a reversible practical capacity of around 160 mAh/g.[31−33] However, this practical capacity corresponds to an extraction/insertion of only one lithium per formula unit. Similarly, preliminary experiments with Li_2MnSiO_4 indicated a reversible insertion/extraction of less than 0.5 lithium ion per formula unit.[28] The low practical capacity was attributed to the poor electronic conductivity of Li_2MnSiO_4, and with a reduction in particle size and coating with conductive carbon, capacities close to 200 mAh/g have been realized recently.[34]

The major drawback of the silicate family is their characteristically low electronic conductivity, which has been shown to be up to 3 orders of magnitude lower than that of $LiFePO_4$.[35] To overcome this obstacle, various solution-based synthesis methods such as sol−gel assisted hydrothermal and refluxing methods have been pursued to obtain nanoparticles of Li_2MSiO_4.[29,33,34,37] However, obtaining a phase-pure material by these methods is a challenge, as most of the synthesis methods produce impurities such as Li_2SiO_3, Fe_3O_4, and Mn_2SiO_4, resulting in low capacities.[33,36]

In this regard, hydrothermal and solvothermal approaches are appealing as they could produce phase-pure materials with unique nanomorphologies[24,25,37−39] We showed recently that the olivine $LiMPO_4$ (M = Mn, Fe, Co, and Ni) can be obtained by microwave-assisted solvothermal (MW-ST) and hydrothermal (MW-HT) methods at < 300 °C within a relatively short reaction time of 5−15 min. This approach not only decreases the manufacture time but also allows the creation of unique nanomorphologies.[13−18] With an aim to obtain phase-pure samples, we present here the microwave-solvothermal synthesis and characterization of carbon-decorated nanostructured Li_2FeSiO_4 and Li_2MnSiO_4.

Experimental Section

Microwave-Solvothermal Synthesis of Li_2MSiO_4. Li_2FeSiO_4 and Li_2MnSiO_4 were prepared by a microwave-solvothermal approach as described below. Appropriate quantities of tetraethyl orthosilicate (TEOS; Acros Organics), lithium hydroxide (Fisher), and iron(II) acetate or anhydrous manganese(II) acetate (STREM Chemicals) or manganese(II) acetate tetrahydrate (Acros Organics) were first dissolved in 30 mL of tetraethyleneglycol (TEG) (ACROS-Organics) and transferred into a quartz vessel suitable to be used in the microwave system. The concentrations of the reactants were kept at 0.30 M for Li^+ and 0.15 M each for Fe^{2+}/Mn^{2+} and $(SiO_4)^{4-}$ in TEG. The homogeneous solutions were then sealed in quartz vessels and placed on a turntable for uniform heating in an Anton Paar microwave irradiation system (Synthos-3000) equipped with a wireless pressure and temperature sensor. The automatic temperature and pressure control system allowed continuous monitoring and control of the internal temperature (±1 °C) and pressure (up to 80 bar). With an operating frequency of 2.45 GHz and a constant power of 600 W for 25 min, the temperature and pressure reached the maximum set value of, respectively, 300 °C and 30 bar after 20 min. Precipitation of Li_2MSiO_4 took place inside the reactor during this solvothermal process, and the reactor was then cooled to

(14) Yamada, A.; Chung, S. C.; Hinokuma, K. *J. Electrochem. Soc.* **2001**, *148*, A224.
(15) Chung, S.−Y.; Bloking, J. T.; Chiang, Y.−M. *Nat. Mater.* **2002**, *1*, 123.
(16) Herle, P. S.; Ellis, B.; Coombs, N.; Nazar, L. F. *Nat. Mater.* **2004**, *3*, 147.
(17) Doeff, M. M.; Hu, Y.; McLarnon, F.; Kostecki, R. *Electrochem. Solid-State Lett.* **2003**, *6*, A207.
(18) Wang, Y.; Wang, J.; Yang, J.; Nuli, Y. *Adv. Funct. Mater.* **2006**, *16*, 2135.
(19) Wang, C. S.; Hong, J. *Electrochem. Solid-State Lett.* **2003**, *10*, A65.
(20) Vadivel Murugan, A.; Muraliganth, T.; Manthiram, A. *Electrochem. Commun.* **2008**, *10*, 903.
(21) Vadivel Murugan, A.; Muraliganth, T.; Manthiram, A. *J. Phys. Chem. C* **2008**, *112*, 14665.
(22) Muraliganth, T.; Vadivel Murugan, A.; Manthiram, A. *J. Mater. Chem.* **2008**, *18*, 5661.
(23) Vadivel Murugan, A.; Muraliganth, T.; Manthiram, A. *Inorg. Chem.* **2009**, *48*, 946.
(24) Yang, S.; Zavalji, P.; Whittingham, M. S. *Electrochem. Commun.* **2001**, *3*, 505.
(25) Ellis, B.; Ka, W. H.; Makahnou, W. R. M.; Nazar, L. F. *J. Mater. Chem.* **2007**, *17*, 3248.
(26) Arunkumar, T. A.; Wu, Y.; Manthiram, A. *Chem. Mater.* **2007**, *19*, 3067.
(27) Nyten, A.; Abouimrane, A.; Armand, M.; Gustafsson, T.; Thomas, J. O. *Electrochem. Commun.* **2005**, *7*, 156.
(28) Dominko, R.; Bele, M.; Gaberščcek, M.; Meden, A.; Remskar, M.; Jamnik, J. *Electrochem. Commun.* **2006**, *8*, 217.
(29) Gong, Z. L.; Li, Y. X.; He, G. N.; Yang, Y. *Electrochem. Solid-State Lett.* **2008**, *11*(5), A60.
(30) Lyness, C.; Delobel, B.; Armstron, A. R.; Bruce, P. G. *Chem. Commun.* **2007**, 4890.
(31) Nyten, A.; Kamali, S.; Haggstrom, L.; Gustafsson, T.; Thomas, J. O. *J. Mater. Chem.* **2006**, *16*, 2266.
(32) Nishimura, A.−I.; Hayese, S.; Kanno, R.; Yashima, M.; Nakayama, N.; Yamada, A. *J. Am. Chem. Soc.* **2008**, *130*(40), 13212.
(33) Dominko, R.; Conte, D. E.; Hanzel, D.; Gaberscek, M.; Jamnik, J. *J. Power Sources* **2008**, *178*, 842.
(34) Li, Y. X.; Gong, J. L.; Yang, Y. *J. Power Sources* **2007**, *174*, 528.
(35) Dominko, R. *J. Power Sources* **2008**, *184*, 462.
(36) Belharouak, I.; Abouimrane, A.; Amine, K. *J. Phys. Chem. C* **2009**, *113*, 20733.
(37) Muraliganth, T.; Vadivel Murugan, A.; Manthiram, A. *Chem. Commun.* **2009**, 7360.
(38) Panda, A. B.; Glaspell, G.; El-Shall, M. S. M. *J. Am. Chem. Soc.* **2006**, *128*, 2790.
(39) Gerbec, J. A.; Magana, D.; Washington, A.; Strouse, G. F. *J. Am. Chem. Soc.* **2005**, *127*, 15791.

room temperature after being maintained at 300 °C for 5 min. The supernatant TEG solvent was carefully decanted, and the resulting Li_2MSiO_4 powder was washed repeatedly with acetone until the washings were colorless to ensure a complete removal of TEG. Because of the sensitivity of the material in air, the obtained powder was then transferred to an argon-filled glovebox.

Synthesis of Li_2MSiO_4/C Nanocomposites. The Li_2MSiO_4 nanocrystals obtained by the microwave assisted solvothermal process were mixed with 30 wt % sucrose powder and carbonized in a flowing argon atmosphere at 650 °C for 6 h to achieve the carbon coating. The carbon content in the composite, thus, obtained was determined to be ~12 wt % by thermogravimetric analysis (TGA). The Li_2MSiO_4 samples heated in Ar atm at 650 °C with and without sucrose were analyzed by heating to 700 °C in air atm (heating and cooling rates of 2 °C/min) in TGA, and the carbon content was calculated from the difference in weight loss between the two samples.

Structural and Chemical Characterizations. X-ray diffraction (XRD) characterizations of the samples were carried out with a Philips X'Pert diffractometer and filtered Cu Kα radiation. Scanning electron microscopy (SEM) and transmission electron microscopy (TEM) characterizations were carried out, respectively, with a JEOL-JSM5610 SEM and a JEOL JEM-2010F equipment. Raman spectroscopic analysis was performed with a Renishaw InVia system utilizing a 514.5 nm incident radiation and a 50× aperture (N.A. 0.75), resulting in approximately a 2 μm diameter sampling cross section. Elemental analyses were carried out with Varian 715-EIS inductively coupled plasma analyzer (ICP).

Electrochemical Characterization. Electrochemical performances were evaluated with CR2032 coin cells with an Arbin battery cycler. The cathodes were prepared by mixing 75 wt % active material (Li_2MSiO_4/C) with 20 wt % conductive carbon and 5 wt % polytetrafluoroethylene (PTFE) binder, rolling the mixture into thin sheets, and cutting them into circular electrodes of 0.64 cm^2 area. The electrode fabrication was carried out in an argon-filled glovebox, as Li_2MSiO_4 has been shown to be unstable in air. The coin cells were fabricated inside the glovebox with the Li_2MSiO_4/C cathode, metallic lithium anode, 1 M $LiPF_6$ in 1:1 diethyl carbonate/ethylene carbonate electrolyte, and Celgard polypropylene separator.

Thermal Stability Characterization. Thermal stability was analyzed with a Netzsch STA 449 F3 differential scanning calorimeter. The cell was first charged to a voltage of 4.7 V and then carefully opened inside a dry glovebox to recover the cathode material. The electrode soaked with the electrolyte was then transferred to a stainless steel sealing pan with a gold foil disk and sealed inside the glovebox. The electrode was then analyzed at a heating rate of 10 °C/min with a nitrogen purge gas.

Results and Discussion

Figure 1 shows the XRD patterns of the as-synthesized and carbon-coated Li_2FeSiO_4 and Li_2MnSiO_4. The XRD patterns of the as-synthesized samples obtained after the MW-ST reaction indicates the formation of monoclinic Li_2FeSiO_4 and Li_2MnSiO_4. However, it is apparent that the peaks are not well-defined, indicating incomplete formation of Li_2MSiO_4. In addition, the as-synthesized samples show Fe_3O_4 and Mn_2SiO_4 impurities, respectively, in the cases of Li_2FeSiO_4 and Li_2MnSiO_4. The XRD patterns of the Li_2MSiO_4/C nanocomposites obtained after

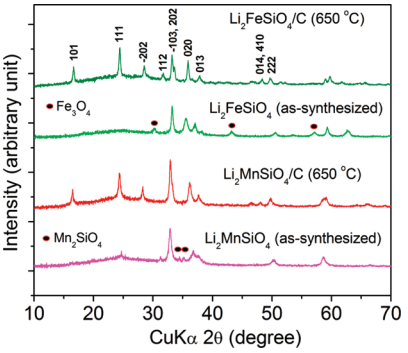

Figure 1. XRD patterns of the as-synthesized and carbon-coated Li_2FeSiO_4 and Li_2MnSiO_4..

heating at 650 °C for 6 h show marked improvement in crystallinity, and all the reflections could be indexed on the basis of the monoclinic structure with the space group *P21*. Thus, heating at 650 °C eliminates the impurity phases and produces a single-phase material.

Li_2MSiO_4 samples were known to crystallize in various polymorphs, depending on the synthesis conditions employed.[30,33] In their initial report, Nyten et al.[27] proposed a β-Li_3PO_4-based structure with $Pmn2_1$ symmetry for Li_2FeSiO_4, where the lithium ions occupy the tetrahedral sites in between the layers comprising chains of alternating corner-shared FeO_4 and SiO_4 tetrahedra running along the *a* direction. However, recent high resolution X-ray diffraction and transmission electron microscopy studies have revealed that the structure can be better refined with a $P2_1$ monoclinic structure with alternating pairs of FeO_4 and SiO_4 tetrahedra, as shown in Figure 2.[32] The lattice parameter values of the $P2_1$ structure were obtained by refining the XRD data with the *CELREF* software. The lattice parameter values of $a = 8.237$ Å, $b = 5.012$ Å, $c = 8.256$ Å, and $\beta = 99.11$ obtained for Li_2FeSiO_4 and $a = 8.228$ Å, $b = 4.983$ Å, $c = 8.265$ Å, and $\beta = 98.41$ for Li_2MnSiO_4 are in close agreement with the literature values.[32] The XRD peaks are broad even after heating to 650 °C due to the nanocrystalline nature of Li_2MSiO_4/C. Further analysis of the XRD data using the Scherrer's formula revealed an average crystallite size of approximately 20 nm for both the Li_2FeSiO_4/C and Li_2MnSiO_4/C samples. The XRD patterns do not show any peaks corresponding to carbon due to its amorphous nature and low content. Elemental analysis of the heated Li_2FeSiO_4 and Li_2MnSiO_4 samples by ICP for lithium, iron, and manganese contents gave a Li/M (M = Fe or Mn) ratio of 2:1, confirming the formation of samples with the Li_2MSiO_4 stoichiometry.

The morphology of the Li_2MSiO_4/C nanocomposites was examined with ultra high resolution field emission scanning electron microscopy (FE-SEM) and high resolution transmission electron microscopy (HR-TEM). Figure 3a−d shows the SEM images of the Li_2FeSiO_4/C and Li_2MnSiO_4/C nanocomposites. Li_2FeSiO_4/C exhibits nanosphere-like morphology with a particle diameter of approximately ~150 nm as seen in Figure 3a. However, when one looks at the magnified SEM image shown in Figures 3b, it becomes apparent that the nanospheres are

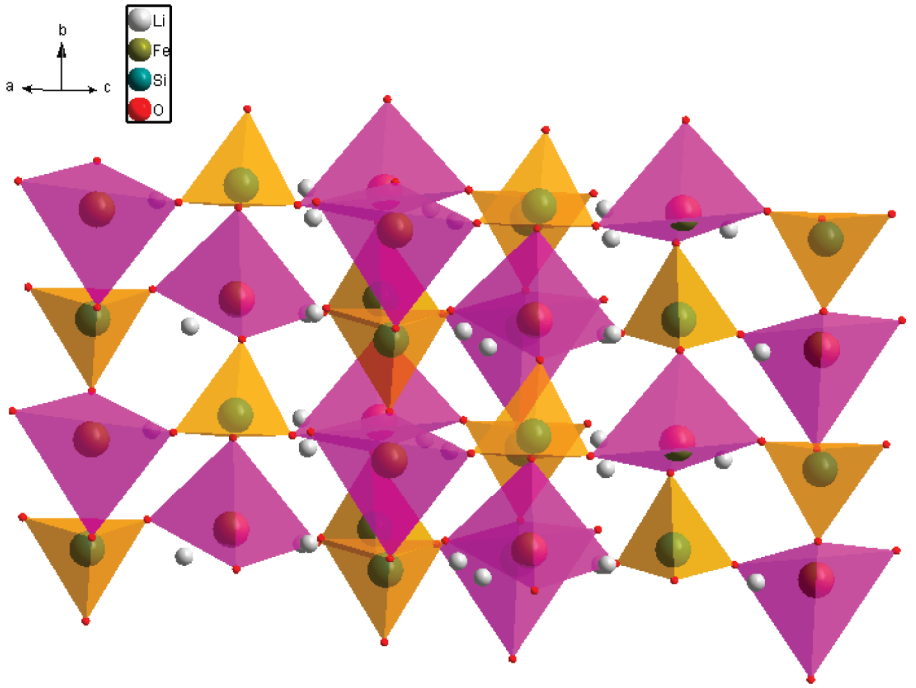

Figure 2. Crystal structure of Li_2FeSiO_4.

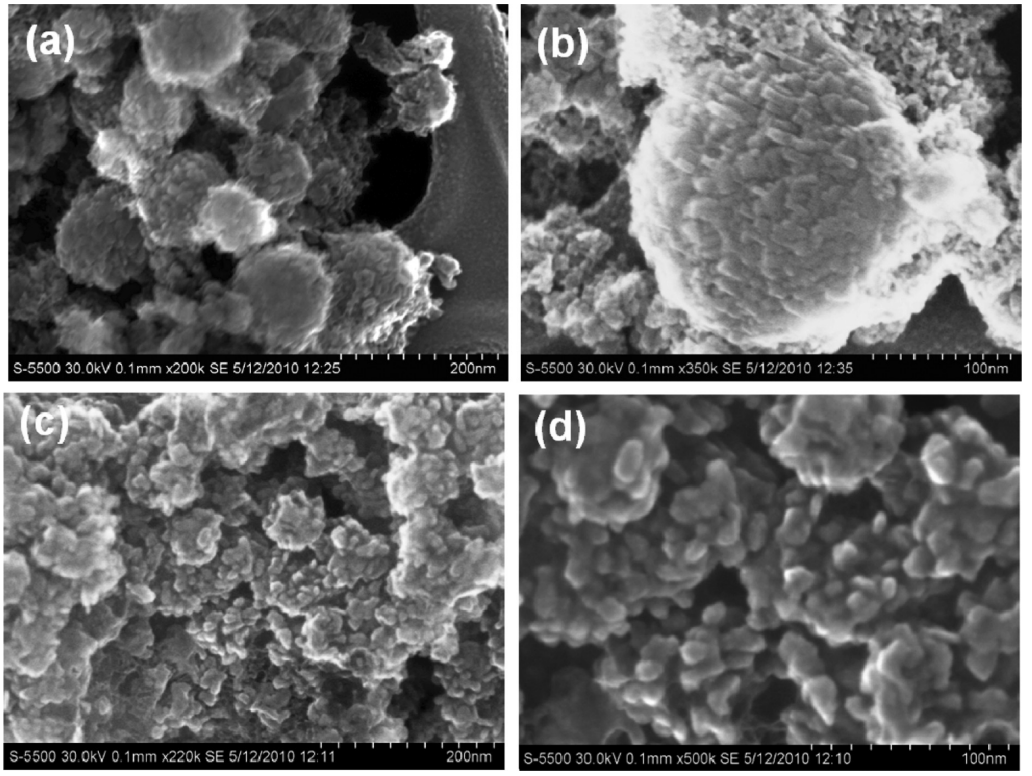

Figure 3. (a) Low and (b) high magnification FE-SEM images of the Li_2FeSiO_4/C nanocomposite and (c) low and (d) high magnification FE-SEM images of the Li_2MnSiO_4/C nanocomposite.

a result of an agglomeration of the nanoparticles of Li_2FeSiO_4 with an average particle size of around 20 nm. Nevertheless, the nanosphere-like morphology is beneficial for increasing the tap density, as the larger size of the secondary particles (~ 150 nm) allows for a denser packing, while the smaller size of the primary particles (~20 nm) improves the lithium-ion and electronic conduction. While Li_2FeSiO_4/C shows nanosphere-like morphology, Li_2MnSiO_4/C shows partially agglomerated nanoparticles with an average particle size of ~20 nm, as seen in Figure 3c,d.

Figure 4a−d shows the TEM and HR-TEM images of the Li_2FeSiO_4/C and Li_2MnSiO_4/C nanocomposites. Figure 4a,c shows the low-magnification TEM images of Li_2FeSiO_4/C and Li_2MnSiO_4/C. Consistent with the

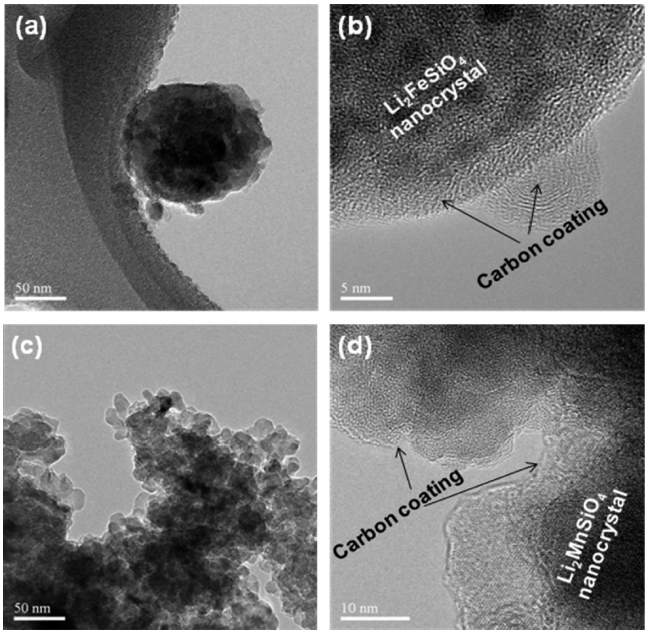

Figure 4. (a) TEM and (b) HRTEM images of the Li_2FeSiO_4/C nanocomposite and (c) TEM and (d) HRTEM images of the Li_2MnSiO_4/C nanocomposite.

SEM images, Li_2FeSiO_4/C adopts a nanosphere-like morphology, while Li_2MnSiO_4/C comprises partially agglomerated nanoparticles. The HR-TEM images in Figure 4b,d shows amorphous carbon coating on the Li_2FeSiO_4 and Li_2MnSiO_4 nanoparticles. Energy dispersive spectroscopic (EDS) data collected in TEM also confirms the presence of uniform carbon coating around the Li_2FeSiO_4 nanocrystals (Supporting Information Figures S1 and S2). The MW-ST method is able to produce nanoparticles because the highly viscous, high boiling point TEG solvent used in the synthesis not only provides a reducing environment to prevent the oxidation of M^{2+} to M^{3+} but also hinders particle growth during the solvothermal synthesis. The small particle size of Li_2MSiO_4 provides short pathways for rapid lithium-ion and electron conduction within the nanoparticles, while the carbon coating connects the nanoparticles in close proximity, providing a highly conductive channel for the electron mobility between adjacent Li_2MSiO_4 nanoparticles.

Raman spectroscopy has emerged in recent years as a powerful tool to characterize sp^2 bonded carbons. Figure 5 shows the Raman spectrum of the Li_2FeSiO_4/C nanocomposite. While the fundamental D and G bands of carbon occur at around, respectively, 1351 and 1603 cm^{-1}, the characteristic bands for Li_2FeSiO_4 are visible around 800 cm^{-1}, all of which attest to carbon-coated Li_2FeSiO_4. The peaks around 800 cm^{-1} correspond to the symmetrically stretching internal vibrational modes of the SiO_4 anions in Li_2FeSiO_4.[40] The carbon spectrum could be deconvoluted into four Gaussian bands at 1603, 1505, 1351, and 1199 cm^{-1}, which are referred to as, respectively, G, D′, D, and I bands,

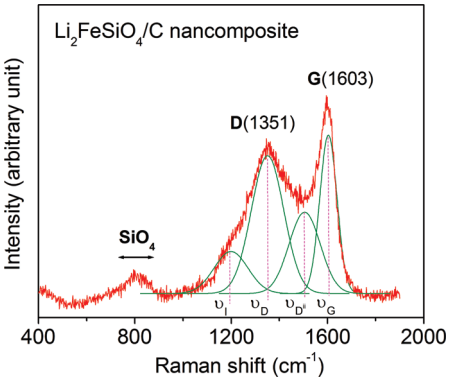

Figure 5. Raman spectrum of the Li_2FeSiO_4/C nanocomposite.

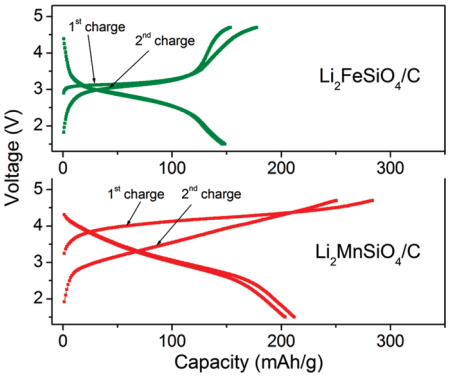

Figure 6. Charge−discharge profiles recorded at C/20 rate and room temperature of Li_2FeSiO_4/C and Li_2MnSiO_4/C.

following the convention of Bonhomme et al.[41] used for peak fitting. The peak intensity ratio between the D and G bands (I_D/I_G) generally provides a useful index for comparing the degree of crystallinity of various carbon materials, i.e., a smaller ratio of I_D/I_G corresponds to a higher degree of ordering in the carbon material. The I_D/I_G ratio for Li_2FeSiO_4 was found to be 1.63, demonstrating that the carbon formed is fairly amorphous due to the low annealing temperature of 650 °C. Thus, the Raman data agree with the TEM images, validating that the carbon coating is amorphous on the Li_2FeSiO_4 nanoparticles. Raman analysis of Li_2MnSiO_4/C also produced similar results.

Galvanostatic charge−discharge measurements were carried out with lithium cells at C/20 rate to evaluate the electrochemical properties of the Li_2MSiO_4/C nanocomposite cathodes. Figure 6 shows the first and second charge−discharge profiles of the Li_2FeSiO_4/C and Li_2MnSiO_4/C nanocomposites at room temperature. The Li_2FeSiO_4/C nanocomposite delivers a first discharge capacity of around 148 mAh/g, which is close to the value expected for the extraction of one lithium per formula unit (166 mAh/g) and the oxidation of Fe^{2+} to Fe^{3+}. The extraction of the second lithium corresponding to the oxidation of Fe^{3+} to Fe^{4+} has been notably absent in previous investigations as well. As seen in Figure 6, the first charge profile shows a nearly flat region around 3.1 V for Li_2FeSiO_4, which occurs at considerably lower potential than that in $LiFePO_4$ (3.43 V).

(40) Zaghib, K.; Ait Salah, A.; Ravet, N.; Mauger, A.; Gendron, F.; Julien, C. M. *J. Power Sources* **2006**, *160*, 1381.
(41) Bonhomme, F.; Lassegues, J. C.; Servant, L. *J. Electrochem. Soc.* **2001**, *148*(11), E450.

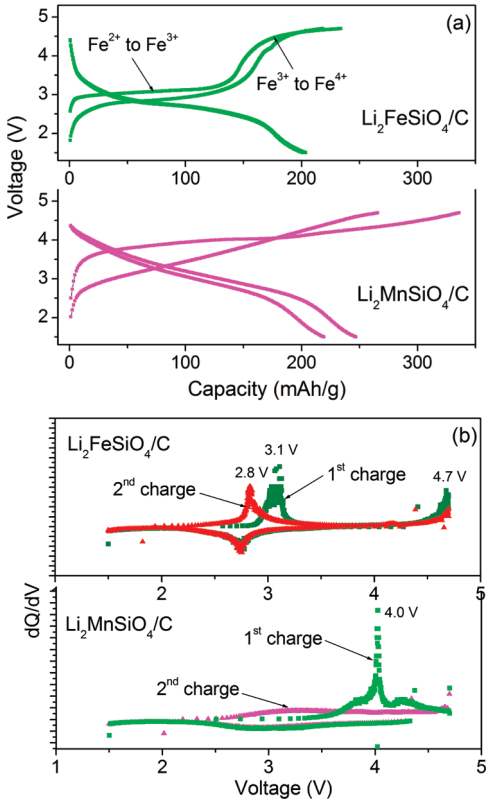

Figure 7. (a) Charge−discharge profiles recorded at C/20 rate and at 55 °C and (b) dQ/dV vs voltage plots of Li_2FeSiO_4/C and Li_2MnSiO_4/C.

It is interesting to note that the second charge curve is different from the first charge curve. This phenomenon has been ascribed to structural rearrangements involving the exchange of lithium and iron between their sites during first charge, as indicated by in situ XRD measurements.[31] In addition, the voltage plateau of the second charge is lower than that of the first charge plateau. However, the first and second discharge curves are similar, implying that there is no major structural change occurring after the first charge. While only close to one lithium ion per formula can be extracted/inserted from/into Li_2FeSiO_4/C, more than one lithium ion per formula could be extracted/inserted from/into Li_2MnSiO_4/C. As seen in Figure 6, Li_2MnSiO_4/C delivers a high first discharge capacity of around 210 mAh/g at C/20 rate at room temperature. Like Li_2FeSiO_4, Li_2MnSiO_4 also shows a decrease in the voltage on going from first charge to second charge.

Figure 7a shows the charge−discharge profiles of Li_2FeSiO_4/C and Li_2MnSiO_4/C at 55 °C. Interestingly, the first charge profile of Li_2FeSiO_4/C exhibits two voltage plateaus corresponding to the $Fe^{2+/3+}$ couple at ~3.1 V and the $Fe^{3+/4+}$ couple at ~4.7 V. Also, the discharge capacity increases significantly from 148 mAh/g at room temperature to 204 mAh/g at 55 °C, demonstrating the ability to extract/insert an additional lithium involving the $Fe^{3+/4+}$ couple at high temperatures. The increase in capacity and lithium extraction at high temperatures can be attributed to enhanced kinetics. As seen in Figure 7a, Li_2MnSiO_4/C also delivers a high charge capacity of around 335 mAh/g and a high discharge capacity of around 250 mAh/g at 55 °C, corresponding to a reversible extraction and insertion of, respectively, about 2 and 1.5 lithium ions per formula unit. Additionally, the polarization loss (voltage difference between the charge and discharge curves) is significantly decreased at high temperatures compared to that at room temperature.

Figure 7b shows the dQ/dV vs voltage plots of Li_2FeSiO_4/C and Li_2MnSiO_4/C. The peaks correspond to the voltage plateaus of the $M^{2+/3+}$ and $M^{3+/4+}$ redox couples. Interestingly, Li_2FeSiO_4 shows two cathodic peaks during first charge, one at ~3.1 V and the other at ~4.7 V, which correspond to the redox reaction involving Li_2FeSiO_4/$LiFeSiO_4$ ($Fe^{2+/3+}$) and $LiFeSiO_4$/$Li_{1-x}FeSiO_4$ ($Fe^{3+/4+}$). In contrast, Li_2MnSiO_4/C shows a single cathodic peak at ~4 V, corresponding to both the $Mn^{2+/3+}$ and $Mn^{3+/4+}$ redox couples. Figure 7b also shows the shift in the cathodic peak from 3.1 V for the first charge to 2.8 V for the second charge in Li_2FeSiO_4, with the anodic peak occurring at the same potential for both the first and second discharge. However, Li_2MnSiO_4/C does not exhibit a sharp peak during discharge, possibly due to structural rearrangements and conversion of the crystalline Li_2MnSiO_4 into an amorphous phase during the first charge.[34]

Figure 8a,b shows the cyclability of the Li_2FeSiO_4/C and Li_2MnSiO_4/C nanocomposite cathodes at room temperature and at 55 °C. Li_2FeSiO_4/C exhibits a stable cycle life with 100% capacity retention at both room temperature and 55 °C, demonstrating its good reversibility and structural integrity during cycling. In contrast, Li_2MnSiO_4/C exhibits drastic capacity fade, especially at 55 °C, and it retains only 50% of its initial capacity at room temperature and 15% of its initial capacity at 55 °C after 20 cycles. This poor capacity retention of Li_2MnSiO_4/C is due to the presence of Mn^{3+} ions, which could lead to dynamic Jahn−Teller distortion and manganese dissolution, as in the case of $LiMn_2O_4$ spinel cathodes.[42,43] The poor cycle performance of Li_2MnSiO_4 can also be ascribed to the structural instability of the delithiated phase, which turns into an amorphous state after the first charge, as indicated by a recent ex situ XRD measurement.[34]

Figure 9 shows the discharge profiles of Li_2FeSiO_4/C and Li_2MnSiO_4/C at various C-rates to illustrate their rate capability. The profiles were recorded by charging the cathodes at the same rate of C/50 and discharging at different rates ranging from C/50 to 2C at room temperature. While Li_2FeSiO_4/C retains about 70% of its capacity on going from C/50 to 2C rate, Li_2MnSiO_4/C retains only around 40% of its capacity. The rate performance of Li_2MnSiO_4/C is worse than that of Li_2FeSiO_4/C due to dynamic Jahn−Teller distortion and lower electronic conductivity (~10^{-16} S/cm) compared to that of Li_2FeSiO_4 (~10^{-14} S/cm).[35] The Li_2FeSiO_4/C sample synthesized by the MW-ST approach exhibit impressive rate

(42) Ohzuku, T.; Kitagawa, M.; Hirai, T. *J. Electrochem. Soc.* **1990**, *137*, 769.
(43) Jang, D. H.; Shin, Y. J.; Oh, S. M. *J. Electrochem. Soc.* **1996**, *143*, 2204.

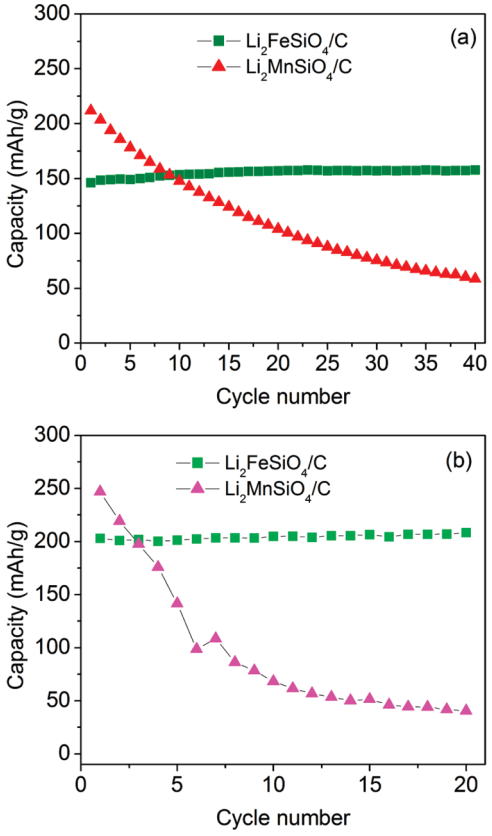

Figure 8. Cyclability data of Li_2FeSiO_4/C and Li_2MnSiO_4/C at (a) 25 °C and (b) 55 °C.

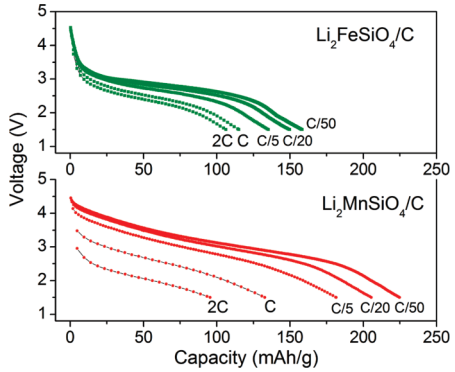

Figure 9. Discharge profiles recorded at different C rates of Li_2FeSiO_4/C and Li_2MnSiO_4/C, demonstrating the rate capability.

performance despite its poor electronic conductivity due to the synergistic effect of short lithium diffusion path length in the small nanoparticles (<20 nm) and the uniform conductive matrix provided by the carbon.

When designing battery electrodes, safety is an important factor to consider. Differential scanning calorimetry (DSC) is a useful technique for comparing the behavior of different electrodes under the conditions of thermal runaway, thus quantifying the relative safety of the electrodes. Accordingly, the cells were charged to 4.7 V prior to analysis because higher states of charge are known to be less stable due to the deintercalated lattice.[44] Figure 10

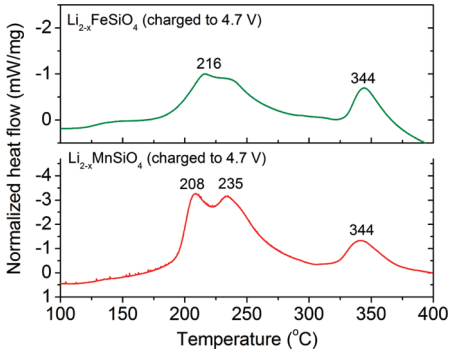

Figure 10. DSC profiles of the charged (to 4.7 V) $Li_{2-x}FeSiO_4$/C and $Li_{2-x}MnSiO_4$/C.

shows the DSC plots for $Li_{2-x}FeSiO_4$ and $Li_{2-x}MnSiO_4$. For $Li_{2-x}FeSiO_4$, two peaks are observed at 216 and 344 °C, with a total exothermic heat flow of 330 J/g. $Li_{2-x}MnSiO_4$ exhibits three peaks at 208, 235, and 344 °C with a total exothermic heat flow of 1060 J/g. Even though the peak temperatures are similar for both the $Li_{2-x}FeSiO_4$ and $Li_{2-x}MnSiO_4$ cathodes, $Li_{2-x}MnSiO_4$ exhibits a 3-fold higher heat flow during the exothermic reaction in DSC. This sizable difference in heat flow between $Li_{2-x}FeSiO_4$ and $Li_{2-x}MnSiO_4$ can be attributed to the fact that there is a high fraction of the higher oxidation state Mn^{4+} in the fully charged $Li_{2-x}MnSiO_4$, whereas the fully charged $Li_{2-x}FeSiO_4$ contains predominantly Fe^{3+}, as evidenced by the differences in the charge capacities in Figure 6. The poor thermal stability of $Li_{2-x}MnSiO_4$ can be further rationalized by considering the structural instability of its delithiated phase. For a comparison, $LiFePO_4$ is reported to have two peaks in the range of 240−360 °C with an exothermic heat flow of 210 J/g.[45] While the thermal stability of Li_2FeSiO_4 is slightly worse than that of $LiFePO_4$, it is much better than that of Li_2MnSiO_4 and layered oxide cathodes. Depending on the composition, layered oxide cathodes have been reported to exhibit peak temperatures between 200 and 310 °C, but the enthalpy of reaction typically ranges from over 1000 to 3300 J/g.[46,47] Consequently, Li_2FeSiO_4 is an attractive candidate for large-scale applications due to its good thermal stability and safety characteristics.

Conclusions

In summary, we have demonstrated the synthesis of carbon-decorated Li_2FeSiO_4 and Li_2MnSiO_4 nanostructures by a novel microwave-solvothermal approach. The nanostructured samples obtained by the MW-ST process provide short pathways for rapid lithium-ion and electronic conduction within the nanoparticles, and the carbon coating improves the electronic conductivity. More importantly, while only one lithium ion has been shown

(44) Joachin, H.; Kaun, T. D.; Zaghib, K.; Prakash, J. *J. Electrochem. Soc.* **2009**, *156*, A401.
(45) Li, G.; Azuma, H.; Tohda, M. *J. Electrochem. Soc.* **2002**, *149*, A743.
(46) Sun, Y.-K; Myung, S.−T.; Park, B.−C.; Prakash, J.; Belharouak, I.; Amine, K. *Nat. Mater.* **2009**, *8*, 320.
(47) Belharouak, I.; Sun, Y.−K.; Liu, J.; Amine, K. *J. Power Sources* **2003**, *123*, 247.

to be reversibly extracted/inserted from/into Li_2FeSiO_4 in previous reports, more than one lithium could be extracted from our Li_2FeSiO_4/C sample at 55 °C, as evidenced by an increase in the discharge capacity to 204 mAh/g. The Li_2FeSiO_4/C sample is also found to exhibit excellent cyclability and rate capability along with good safety characteristics. Although Li_2MnSiO_4/C displays high capacities of around 210 and 250 mAh/g at 25 and 55 °C, it exhibits poor rate performance and drastic capacity fade during cycling. The poor capacity retention and rate performance can be ascribed to Jahn−Teller distortion, structural instability, and low electronic conductivity. Additionally, Li_2MnSiO_4 displays poor thermal stability, as shown by the DSC data.

Acknowledgment. This work was supported by the Office of Vehicle Technologies of the U.S. Department of Energy under Contract No. DE-AC02-05CH11231 and Welch Foundation Grant F-1254.

Supporting Information Available: TEM-EDS analysis of Li_2FeSiO_4/C nanocomposites (PDF). This material is available free of charge via the Internet at http://pubs.acs.org.